Article

Chinese Science Bulletin

Materials Science

May 2012 Vol.57 No.13: 1595–1599
doi: 10.1007/s11434-012-5024-3

Electromagnetic modification of faceted-faceted $Ni_{31}Si_{12}$-Ni_2Si eutectic alloy

LU YiPing[1*], LI GuoBin[2], DU YanYan[1], JI YanShuo[1], JIN Qun[1] & LI TingJu[1]

[1] *School of Materials Science and Engineering, Dalian University of Technology, Dalian 116024, China;*
[2] *Marine Engineering College, Dalian Maritime University, Dalian 116026, China*

Received August 26, 2011; accepted September 28, 2011; published online March 8, 2012

In an electromagnetic field, the morphology of a binary faceted-faceted (FF) $Ni_{31}Si_{12}$-Ni_2Si eutectic microstructure and the alloy's mechanical properties were investigated. Hardness experiments demonstrated that the solidified ingots were significantly strengthened, and the hardness was improved to 63.1 and 786.6 on the Rockwell hardness C and Vickers hardness scales, respectively. Tests of friction and wear in stirred FF eutectic alloys showed excellent anti-fatigue and anti-adhesion wear performance. Alloy changed from an anomalous microstructure to a refined quasi-regular structure, and there was an increase in the lamellar microstructure fraction. The formation process of the refined quasi-regular microstructure and the resulting mechanical properties were investigated.

eutectic alloy, electromagnetic field, microstructure, mechanical properties

Citation: Lu Y P, Li G B, Du Y Y, et al. Electromagnetic modification of faceted-faceted $Ni_{31}Si_{12}$-Ni_2Si eutectic alloy. Chin Sci Bull, 2012, 57: 1595–1599, doi: 10.1007/s11434-012-5024-3

According to Jackson's theory [1,2], binary eutectic systems can be classified into three groups based on their solution entropies ΔS [3,4] as follows. (1) The microstructure will be regular if for both phases $\Delta S \leqslant 23$ J/(mol K); this is the non-faceted–non-faceted (NN) group. (2) The microstructure will be complex–regular, broken lamellar, and/or irregular if one phase has $\Delta S \leqslant 23$ J/(mol K) and the other phase has $\Delta S \geqslant 23$ J/(mol K); this is the faceted–non-faceted (FN) group. (3) The microstructure will be irregular if both phases have $\Delta S \geqslant 23$ J/(mol K); this is the faceted-faceted (FF) group. Eutectic alloys of types (1) and (2) are widely used in various industrial fields. Theoretical research on the solidification mechanisms of such alloys shows that most NN and FN eutectic alloys can obtain regular lamellar or rod-like eutectic structures when they solidify under near-equilibrium condition [5–7].

However, the third type of binary eutectic alloy, i.e. FF eutectic alloys, has rarely been investigated. These alloys generally consist of two intermetallic compounds [8,9]. As a result of the long-range ordered superlattice structures of intermetallic compounds, their metallic bonds are strong. FF eutectic alloys therefore have some special physical, chemical, and mechanical properties, such as high hardness and melting points, low thermal expansion coefficients, and excellent thermal conductivity [10–12]. New materials with these features can be used in the transport, chemicals, machinery, and many other industries. For instance, the binary FF Si-$TaSi_2$ eutectic alloy is used in field-emission materials [13]. The hardness and strengths of some other binary FF eutectic alloys remain unchanged with increasing temperature. The Mo_5Si_3-$MoSi_2$ alloy is a case in point. At temperatures near 1400°C, the strength, thermal conductivity, electrical conductivity, and high-temperature oxidation resistance remain excellent, although these properties fail in other common alloys; this makes it extremely competitive among new high-temperature coating materials [14,15].

For high solution entropies, anisotropic growth of the eutectic phase is strong in the solidification process and the solidified structure is extremely complex. It is very difficult for such eutectic alloys to achieve a regular structure under

*Corresponding author (email: luyiping@dlut.edu.cn)

conventional solidification conditions because the solidified structure is generally loose, and the toughness and plasticity are poor. It is therefore difficult to process this type of eutectic alloy into bars, wire rods, plates, etc. If we can obtain a refined and uniform solidified structure, the toughness and plasticity will be improved. This will greatly reduce the processing costs and increase the use of binary FF eutectic alloys.

Regular microstructures have been obtained in FF $Ni_{31}Si_{12}$-Ni_2Si eutectic alloys by rapid solidification [8]. However, it is hard to make large ingots by rapid solidification methods [16]. Although inoculation (i.e. including elements such as B, Ti, and rare-earth elements) can also be used to refine solidified structures, this is sometimes harmful in recycled products, and can increase costs [17].

The use of an electromagnetic field is a good way to refine solidified structures, minimize macro-segregation, and reduce flaws in casting billets, and this method is widely used in various industrial processes involving liquid metals [16–20]. However, there have as yet been no reports of electromagnetic modifications of FF eutectic alloys. FF $Ni_{31}Si_{12}$-Ni_2Si eutectic alloys have potential applications under high-temperature conditions, so we tried to obtain refined or quasi-regular microstructures of binary FF $Ni_{31}Si_{12}$-Ni_2Si eutectic alloys using rotary magnetic fields.

1 Experimental procedures

Master alloys of $Ni_{31}Si_{12}$-Ni_2Si were prepared from 99.99% pure Ni and 99.9999% pure Si by alloying in an arc furnace filled with argon gas of purity 99.99%. Before preheating, the inner surface of an austenitic-steel crucible was coated with ZrO_2, which aids separation of the casting ingot and crucible. The austenitic-steel crucible was placed at the middle of an electromagnetic stirrer, which was located in a VIM-10 modified vacuum-induction furnace. The experimental facilities (VIM-10 modified vacuum-induction furnace) consist of a vacuum median frequency induction furnace, induction transformers, and rotary electromagnetic stirrers. In the experiments, the currents of the rotary electromagnetic stirrers were 60, 80, 100, 120, and 150 A. The master alloys were melted in the VIM-10 modified vacuum-induction furnace. Approximately 3 kg of master alloy were melted, superheated, and poured into an austenitic-steel crucible 250 mm in length, and with upper inner diameter Φ82 mm and bottom inner diameter Φ70 mm. The superheated temperature and the pouring temperature were kept at 1638 K. An electromagnetic field with frequency 50 Hz was imposed. Some ingots were cast in the absence of a rotary magnetic field. In all cases, the vacuum was evacuated to 6×10^{-2} Pa and backfilled to 6×10^4 Pa with high-purity argon gas during the melt treatment. An IRTM-2CK infrared pyrometer was used to measure the temperature with an absolute accuracy of ±2 K. The microstructures of the solidified samples were investigated by optical microscopy (OM) and laser scanning confocal microscopy (OLYMPUS-TY8648 LSCM). The ingots were cut into two halves along the symmetry axis. One half was mounted in an epoxy material, sectioned, polished, and etched with a mixture of 50 mL of water, 3 mL of hydrofluoric acid, and 3 mL of hydrogen peroxide.

Hardness measurements on the polished specimens were carried out using a Vickers pyramid hardness (HV) testing machine (model number: MH-6) and a Rockwell hardness (HRC) tester (model number: TH-300). The indentation load and time were 500 g and 15 s, respectively, in the HV tests, and 150 kg and 15 s, respectively, in the HRC tests. Every sample was measured five times, and the average value was used.

Unduplicated friction and wear experiments were performed under laboratory conditions (293 K, 45% relative humidity) using the wear tester (model number: MMW-1-type) shown in Figure 1. The upper part of the tester is a special jig (8). A ball sample (9) is fixed to the jig so that it can rotate synchronously with the principal axis (7), which is connected to the electromotor of the ball-on-disc tester. During the test, the ball sample (9) slides on the disc (circular)

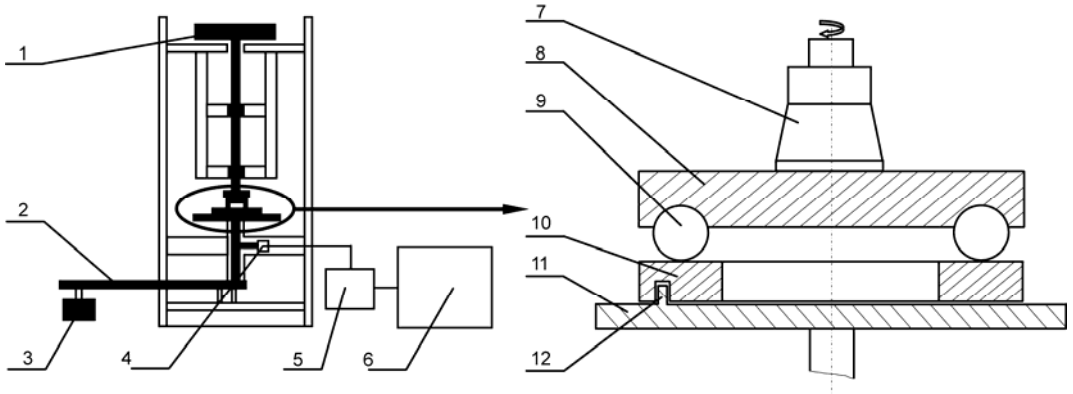

Figure 1 Schematic illustration of MMW-1-type tester. (1) Electromotor; (2) active system; (3) weight; (4) friction moment sensor; (5) data acquisition system; (6) computer; (7) principal axis; (8) special jig; (9) ball sample; (10) disc sample; (11) support of disc sample; (12) locating pin.

sample (10), which is fixed by another jig (11). A locating pin (12), of size of Φ2 mm × 3 mm, is used to keep the disc sample (10) and the jig (11) coaxial. The rotation speed of the wear tester ranges from 0 to 2000 r/min and the load ranges from 0 to 1000 N. The friction force can be recorded online during testing by a sensor and computer connected to the tester. In this study, a ceramic ball of diameter of 12.7 mm was selected as the ball sample and its surface hardness was HV1500. The stirred FF eutectic alloys were used for disk samples of size of Φ31.7 mm × 10 mm. The rotation speed of the ball sample was 100 r/min and its sliding velocity was 0.375 m/s. The test load was 100 N and the contact pressure was 0.8 MPa. The test duration was 20 min. All samples were ultrasonically cleaned and then dried before the wear tests.

2 Results and discussion

Around the eutectic composition of 29.8% Si, the ordered intermetallic compound γ ($Ni_{31}Si_{12}$) and δ (Ni_2Si) phases are formed in an equilibrium eutectic reaction [21], by initiating the 50-Hz/120-A electromagnetic field as soon as the molten metal was poured into the austenitic-steel crucible. When the current is lower than 120 A, the solidified microstructure is coarser. Although better refinement of the microstructures of FF alloys is achieved by increasing the current, this produces more waste materials and rough edges. So, a current of 120 A was finally chosen, after repeatedly adjusting the current and comparing the samples.

Figure 2 shows the microstructures of FF $Ni_{31}Si_{12}$-Ni_2Si eutectic alloys processed with/without the electromagnetic field. The microstructures of the FF $Ni_{31}Si_{12}$-Ni_2Si eutectic alloy processed without the electromagnetic field are heterogeneous, as shown in Figure 2a. The bright cell phase is γ ($Ni_{31}Si_{12}$) and a lamellar structure of both, i.e. γ and δ phases forms between the cells (Figure 2a). From Figure 2b, it can be seen that the middle part of the bulk ingot of the FF $Ni_{31}Si_{12}$-Ni_2Si eutectic alloy has a homogeneous lamellar microstructure in the presence of an electromagnetic field. However, a dendritic eutectic of thickness ~5 mm (measured from the center point) was observed in the upper part of the ingots. A mixture of a lamellar microstructure and a refined primary γ phase was observed at the bottom of the ingot, with a thickness of ~8 mm. This is because the primary $Ni_{31}Si_{12}$ phase protruding from the solid-liquid interface during the coupled growth was scoured, broke off, and segregated to the top and bottom of the ingots under the action of electromagnetic stirring.

By comparing Figure 2a and b, we can see that the electromagnetic field obviously refines/reduces the primary γ phases, and also increases the fraction of lamellar microstructures. In the presence of an electromagnetic field, forced convection can cause primary γ cell fragmentation and melting of the fragments, accelerate solute diffusion, and reduce the temperature gradient G and solute undercooling. This increases the heterogeneous nucleation rate and promotes the development of lamellar microstructures, thereby increasing the fraction of lamellar microstructures.

To gain a better understanding of the mechanical properties of FF $Ni_{31}Si_{12}$-Ni_2Si eutectic alloys, their macro-hardness and micro-hardness were investigated. The HV and HRC values of $Ni_{31}Si_{12}$-Ni_2Si eutectic alloys processed with/without an electromagnetic field are displayed in Table 1. It can be seen that both the HV (786.6) and HRC (63.1) of FF $Ni_{31}Si_{12}$-Ni_2Si eutectic alloys with an electromagnetic field are higher than the HV (667.2) and HRC (57.9) of FF $Ni_{31}Si_{12}$-Ni_2Si eutectic alloys without an electromagnetic field. The HV and HRC values of $Ni_{31}Si_{12}$-Ni_2Si eutectic alloys with an electromagnetic field improved by 17.9% and

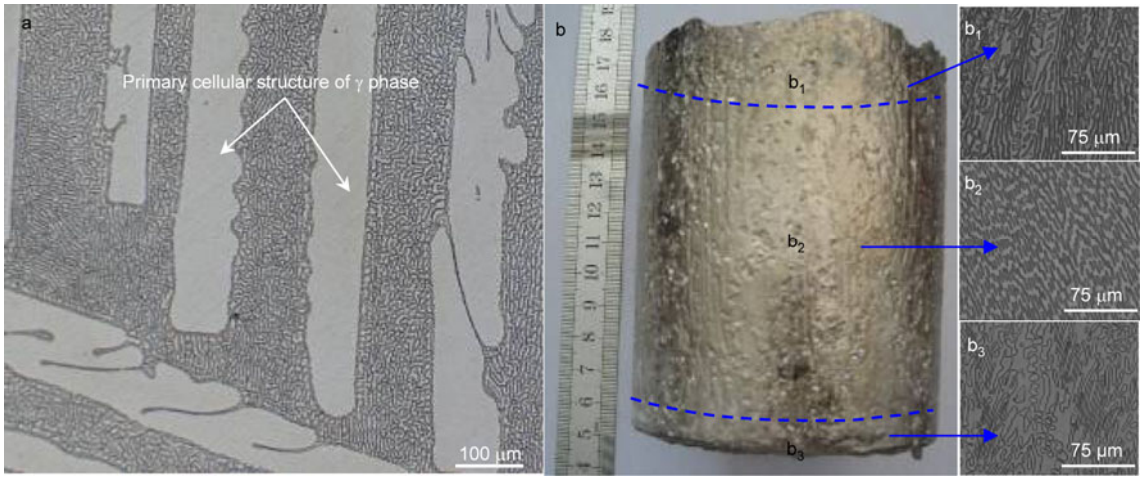

Figure 2 Microstructure of FF $Ni_{31}Si_{12}$-Ni_2Si eutectic alloy under different conditions: a, without an electromagnetic field; b, with an electromagnetic field, I = 120 A; b_1, dendritic eutectic microstructure observed in the upper part of the ingots, of thickness ~5 mm (measured form the center point); b_2, refined lamellar microstructure observed within the ingot; b_3, mixture of lamellar and refined primary γ phase observed at the bottom of the ingot, with a thickness of ~8 mm.

Table 1 Hardness values of FF $Ni_{31}Si_{12}$-Ni_2Si eutectic alloy with/without an electromagnetic field

Test times		1	2	3	4	5	Average
With electromagnetic	HV	786	788	778	772	809	786.6
	HRC	64.5	63.5	62	64	63.5	63.1
Without electromagnetic	HV	680	655	630	711	660	667.2
	HRC	57.8	57	58.2	57.5	59	57.9

9%, respectively.

Figure 3 shows the surface morphologies of stirred FF eutectic alloys. It can be seen that the large pits and grooves on the surface disappear after wear tests. The reasons for surface damage include plastic deformation (marked by B), small fatigue cracks (marked by C), and shedding of abrasive particles (marked by A). The variations in friction coefficient μ with wear time are shown in Figure 4. There is no obvious change in the friction coefficient and it tends to remain constant during sliding. The properties of the worn surfaces and the variations in friction coefficient indicate that the wear mechanism of stirred FF eutectic alloys is steady abrasive wear, and that stirred FF eutectic alloys are characterized by anti-fatigue and anti-adhesion wear.

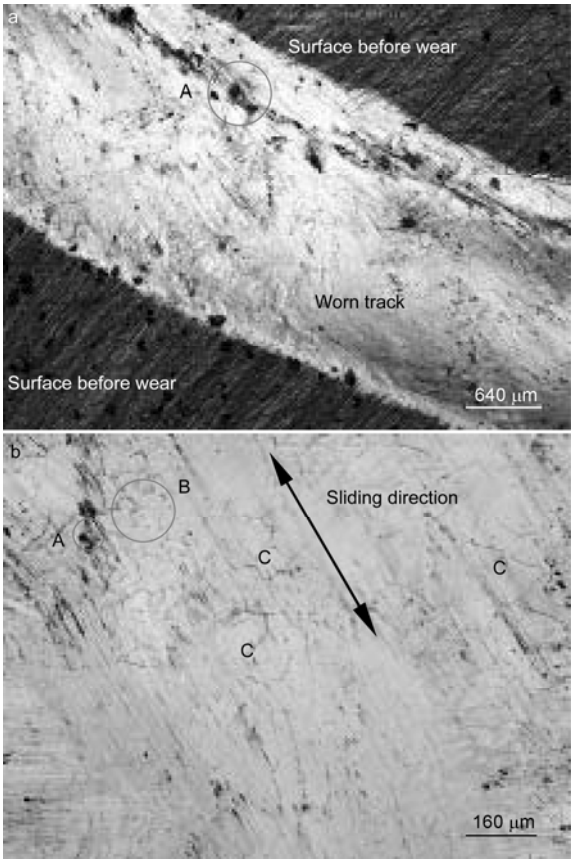

Figure 3 Laser scanning confocal microscopy (LSCM) images of wear surface for the stirred FF eutectic alloy sample.

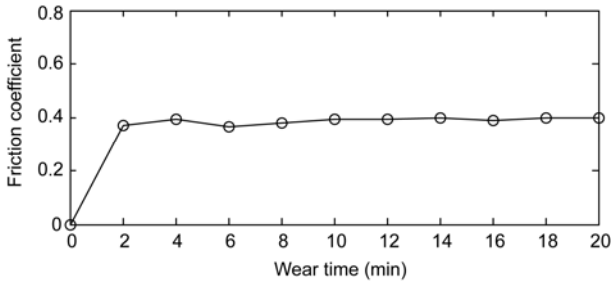

Figure 4 Variations in friction coefficient μ with wear time.

3 Conclusions

In summary, the microstructures and mechanical properties of FF $Ni_{31}Si_{12}$-Ni_2Si eutectic alloys were investigated during solidification under an electromagnetic field. A significant change in the morphology of the FF $Ni_{31}Si_{12}$-Ni_2Si eutectic alloy, from an anomalous (coarse cell plus lamellar) microstructure to a refined quasi-regular microstructure, and an increased lamellar microstructure fraction was observed after stirring. This morphology change in the $Ni_{31}Si_{12}$-Ni_2Si eutectic alloy is ascribed to the growth of the primary γ ($Ni_{31}Si_{12}$) phase by restraint, disintegration, and increased nucleation rates caused by the electromagnetic field. Stirred ingots solidified under strong internal melt convection using a 50-Hz frequency rotary magnetic field exhibit an obvious improvement in hardness and excellent anti-fatigue and anti-adhesion wear properties. Stirred FF eutectic alloys have several potential applications because of their special mechanical properties.

This work was supported by the National Natural Science Foundation of China (51104029), the China Postdoctoral Science Foundation Funded Project, and the Fundamental Research Funds for the Central Universities. The authors are grateful to Dr. Li Xiong and Gong Yue for looking over the paper and revising the grammar.

1 Jackson K A. Growth and Perfection of Crystals. New York: John Wiley and Sons Inc, 1958. 319–324
2 Jackson K A. Liquid Metals and Solidification. Cleveland: AM Soc Metal, 1958. 174–176
3 Taylor M R, Fidler R S, Smith R W. The classification of binary eutectics. Metall Trans A, 1971, 2: 1793–1798
4 Fidler R S, Croker M N, Smith R W. The thermodynamics and morphologies of eutectics containing compound phases. J Cryst Growth, 1972, 13/14: 739–746
5 Lu Y P, Xi Z Z, Yang G C, et al. Entropy as a selection rule for crystal growth in undercooled binary eutectic melts. Chin Sci Bull, 2009, 54: 1012–1018
6 Croker M N, Fidler R S, Smith R W. The characterization of eutectic structures. Proc R Soc Lond, 1973, A335: 15–37
7 Croker M N, Baragar D, Smith R W. Anomalous eutectic growth: II. The relationship between faceted/non-faceted eutectic structures. J Cryst Growth, 1975, 30: 198–212
8 Lu Y P, Lin X, Yang G C, et al. The formation of quasi-regular microstructure in highly undercooled $Ni_{70.2}Si_{29.8}$ eutectic alloy. J App Phys, 2008, 104: 013535
9 Lu Y P, Liu F, Yang G C, et al. Composite growth in highly under-

cooled $Ni_{70.2}Si_{29.8}$ eutectic alloy. Appl Phys Lett, 2006, 89: 241902
10 Zhang Y G, Han Y F, Chen G L, et al. Structural Intermetallics. Beijing: National Defence Industrial Press, 2001. 2–4
11 Liu G J, Sun J R, Lin J, et al. Entropy changes due to the first-order phase transition in the $Gd_5Si_xGe_{4-x}$ system. Appl Phys Lett, 2006, 88: 212505
12 Lee N T S, Tan V B C, Lim K M. Structural and mechanical properties of Sn-based intermetallics from *ab initio* calculations. Appl Phys Lett, 2006, 89: 141908
13 Cui C J, Zhang J, Jia Z W, et al. Microstructure and field emission properties of the Si-$TaSi_2$ eutectic *in situ* composites by electron beam floating zone melting technique. J Cryst Growth, 2007, 310: 71–77
14 Dai Q X. Metal Material Science. Beijing: Chemical Industry Press, 2006. 248–251
15 Mason D P, Aken D C V, Mansfield J F. On the microstructure and crystallography of directionally solidified $MoSi_2$-Mo_5Si_3 eutectics. Acta Metall Mater, 1995, 43: 1189–1199
16 Wang H P, Chang J, Wei B. Measurement and calculation of surface tension for undercooled liquid nickel and its alloy. J Appl Phys, 2009, 106: 033506
17 Wang H P, Wei B. Density and related thermo physical properties of metastable liquid Ni-Cu-Fe ternary alloys. Phys Lett A, 2010, 374: 2489–2493
18 Wang Q, Li D G, Wang K, et al. Effects of high uniform magnetic fields on the diffusion behavior at Cu/Al solid/liquid interface. Scripta Mater, 2007, 56: 485–488
19 Wang H P, Wei B. Surface tension and specific heat of $Ni_{70.2}Si_{29.8}$ alloy. Chin Sci Bull, 2005, 50: 945–949
20 Hui L, Wang H P, Xie W J, et al. Electrostatic levitation under single-axis feedback control condition. Sci China Phys Mech Astron, 2010, 53: 1438–1444
21 Acker J, Bohmhammel K. Thermodynamic properties of the nickel silicide NiSi between 8 and 400 K. Thermochim Acta, 1999, 337: 187–193